22nd Applied Aerodynamics Conference and Exhibit
Aug 16–19, 2004/Rhode Island

Calculations of Unsteady Flow and Flutter by an Euler and Integral Boundary-Layer Method on Cartesian Grids

Zhichao Zhang* and Feng Liu†
Department of Mechanical and Aerospace Engineering
University of California, Irvine, CA 92697-3975

David M. Schuster‡
Aeroelasticity Branch
NASA Langley Research Center, Hampton, VA 23681

This paper presents an Euler and boundary-layer method capable of unsteady flow and aeroelastic simulations. An integral boundary-layer solver is coupled with an Euler solver in a "semi-inverse" manner. For the inviscid part, approximate wall boundary-conditions are implemented on non-moving mean chord positions, whereas the full nonlinear Euler equation is solved in the field for accurate resolution of shock waves and vorticity. Stationary Cartesian grids are used for both steady and unsteady calculations. An integral boundary-layer method using Green's lag equation is coupled with the outer inviscid flow. Results of steady and unsteady calculations by this interactive boundary-layer method are presented and compared with experimental data. Flutter-boundary predictions for the 2D Isogai wing model are provided and compared with results using the Euler solver without the boundary-layer corrections and also thin-layer Navier-Stokes results. It shows that viscous effects are significant for this case.

I. Introduction

Computational Fluid Dynamics (CFD) has proven to be a useful tool for the simulation and prediction of many unsteady phenomena of aeroelastic systems such as buffet, flutter, and Limit Cycle Oscillation (LCO). Methods ranging from the linear doublet-lattice method[1] to methods that solve the Euler and the Navier-Stokes equations have been developed.[2–7] Despite its limit in handling transonic and other nonlinear flows, the linear doublet-lattice method has been and is still the workhorse for actual design analysis in industry because of its efficiency in computer time and, perhaps equally important, the ease in setting up the computational problem. The Reynolds-Averaged-Navier-Stokes (RANS) methods encompass the most complete flow model short of Large-Eddy-Simulations (LES) or Direct-Numerical-Simulations (DNS). However, RANS simulations for aeroelasticity problems at present demand undesirably large amounts of computational resources in a design environment. In addition, their usefulness is hampered by uncertainties

*Graduate student, AIAA member.
†Professor. Associate Fellow AIAA.
‡Senior Research Engineer. Associate Fellow AIAA

in turbulence modeling, grid resolution, and numerical damping effects;[6,7] difficulties in grid generation and the transfer of displacements and aerodynamic forces between the structural and aerodynamic grids; and lack of fast and robust algorithms for deforming grids needed in the unsteady computations. In between the above two extremes, methods based on the various forms of the potential flow equation with boundary-layer corrections have shown good results for unsteady calculation without the use of large computational resources and with less human work in setting up the computational problem including grid generation. Among such methods, the CAP-TSD[8–10] code is widely known and used. The CAP-TSD code has many advantages over a full-fledged RANS code. These include 1) ease in generating a grid; 2) no need to do complex interpolation between the structural and CFD grids; 3) no need to have a moving grid; 4) less demand on CPU time and memory.

Despite the use of vortex and entropy corrections, the potential flow assumption in CAP-TSD limits its applicability to irrotational flows with weak shocks. On the other hand, Euler methods are capable of resolving strong shocks and transporting vortices correctly, and advances in computer speed and maturity of algorithms for the Euler equations have made the solution of the Euler equations a rather dependable and routine tool. Due to the requirement of large computing resources by a Navier-Stokes code and also unresolved issues regarding accuracy of current numerical algorithms for the Navier-Stokes equations, the Euler method with boundary layer coupling provides a good balance between completeness of the flow model and computational efficiency. In fact, interactive boundary-layer methods using the Euler equations have already been investigated by many researchers.[11–14] However, most of them focus on steady calculations.

In order to retain the ease in setting up a computational grid as in the CAP-TSD code, we use the efficient time-accurate Cartesian Euler solver developed by Gao et al.[15] to solve the outer inviscid flow. For the viscous part, we employ an integral boundary-layer method using Green's lag equation.[16] This coupling method of Cartesian Euler with integral boundary-layer in a "semi-inverse" manner is very convenient and efficient for the calculation of unsteady transonic flow around airfoils.

We first describe the unsteady Cartesian Euler method, the integral boundary-layer method and the inviscid-viscous coupling scheme. Then numerical examples of steady and unsteady calculations including flutter boundary predictions are presented and the results are compared with experimental data or other numerical results. Discussions and conclusions are finally drawn.

II. Time-Accurate Euler Method on a Cartesian Grid

The two-dimensional unsteady Euler equations in conservative integral form over a fixed control volume V enclosed by the surface S are:

$$\frac{\partial}{\partial t}\int_V \mathbf{W} dV + \int_S \mathbf{G}\cdot\mathbf{n} dS = 0 \tag{1}$$

where

$$\mathbf{W} = \begin{bmatrix} \rho \\ \rho u \\ \rho v \\ \rho E \end{bmatrix} \tag{2}$$

$$\mathbf{G} = \begin{bmatrix} \rho\mathbf{q} \\ \rho u\mathbf{q} + p\mathbf{e}_x \\ \rho v\mathbf{q} + p\mathbf{e}_y \\ \rho E\mathbf{q} + p(u\mathbf{e}_x + v\mathbf{e}_y) \end{bmatrix} \tag{3}$$

$$\mathbf{q} = u\mathbf{e}_x + v\mathbf{e}_y \tag{4}$$

$$E = \frac{1}{\gamma - 1}\frac{p}{\rho} + \frac{1}{2}(u^2 + v^2) \tag{5}$$

Applying (1) to each cell in the mesh we obtain a set of ordinary differential equations of the form

$$\frac{d}{dt}(\mathbf{W}_{i,j}V_{i,j}) + \mathbf{R}(\mathbf{W}_{i,j}) = 0 \tag{6}$$

where $V_{i,j}$ is the volume of the i,j cell and the residual $\mathbf{R}(\mathbf{W}_{i,j})$ is obtained by evaluating the flux integral in (1). Following Jameson,[17] we approximate the $\frac{d}{dt}$ operator by an implicit backward difference formula of second-order accuracy in the following form (dropping the subscripts i,j for clarity)

$$\frac{3}{2\Delta t}[\mathbf{W}^{n+1}V] - \frac{2}{\Delta t}[\mathbf{W}^{n}V] + \frac{1}{2\Delta t}[\mathbf{W}^{n-1}V] + \mathbf{R}(\mathbf{W}^{n+1}) = 0 \tag{7}$$

Eqn. (7) can be solved for $\mathbf{W}^{n+1}$ at each time step by solving the following steady-state problem in a pseudo time t^*.

$$\frac{d\mathbf{W}}{dt^*} + \mathbf{R}^*(\mathbf{W}) = 0 \tag{8}$$

where

$$\mathbf{R}^*(\mathbf{W}) = \mathbf{R}(\mathbf{W}) + \frac{3}{2\Delta t}(\mathbf{W}V) - \frac{2}{\Delta t}(\mathbf{W}^{n}V) + \frac{1}{2\Delta t}(\mathbf{W}^{n-1}V) \tag{9}$$

Eqn.(8) is solved by an explicit time-marching scheme in t^* for which the local time stepping, residual smoothing, and multigrid techniques[18] can be used to accelerate convergence to a steady state.

Gao et al.[15] applied the above time-accurate Euler scheme on stationary Cartesian grids for unsteady calculations using a small-perturbation boundary treatment. We briefly describe their method here and the readers are referred to their original paper for details.

A thin airfoil slightly moving or deforming about its mean position is considered. For unsteady calculations in the present paper, the airfoil is assumed to be of rigid shape but performs pitching or plunging motion. The mean position of the airfoil chord lies on the horizontal axis x of the coordinate system between $x = 0$ and $x = 1$. The velocity of the incoming uniform free stream makes an angle α_m with the x axis. The shape of the airfoil is described by $y = f(x)$ and $g(x)$ for its upper and lower surfaces, respectively. The instantaneous position of the airfoil is described by $y = F(t,x)$ and $y = G(t,x)$ for the upper and lower surfaces, respectively. Under the assumption, $|F| \ll 1$, the first-order approximation of the boundary conditions on the upper surface of the airfoil at an instant t is

$$v(t,x,0) = u(t,x,0)F_x + F_t + O(F) \tag{10}$$

where the subscripts, x and t denote the partial derivatives with respect to x and t, respectively; $O(F)$ represents terms of the same order of magnitude as F or higher. The normal velocity boundary condition on the lower surface is treated similarly.

There are altogether four independent variables in the Euler equations (1), e.g. ρ, u, v and p. In addition to the boundary condition for the normal velocity v given above, three more conditions are needed on the airfoil surfaces. Among them, ρ and u can be simply extrapolated from the first several cells adjacent to the wall, whereas p need to be calculated using the normal momentum equation. The momentum differential equation in the outward normal direction $\mathbf{n}$ is

$$\mathbf{n} \cdot [\frac{\partial \mathbf{q}}{\partial t} + (\mathbf{q} \cdot \nabla)\mathbf{q}] = \mathbf{n} \cdot (-\frac{\nabla p}{\rho}) \tag{11}$$

On the upper surface of the airfoil, $y = F(t,x)$, the above equation becomes

$$p_y(t,x,F) = F_x p_x(t,x,F) - \rho(t,x,F)[F_{tt} + 2F_{tx}u(t,x,F) + F_{xx}u^2(t,x,F)] \tag{12}$$

The first-order approximation of the above equation is

$$p_y(t,x,0) = F_x p_x(t,x,0) - \rho(t,x,0)[F_{tt} + 2F_{tx}u(t,x,0) + F_{xx}u^2(t,x,0)] + O(F) \tag{13}$$

The corresponding equations on the lower surface of the airfoil are similarly derived.

For airfoil pitching, the instantaneous angle from the mean position is $\alpha_1(t)$, positive in clockwise direction. Given $f(x)$, the instantaneous ordinate of the upper surface, $F(t,x)$, is expressed implicitly as follows.

$$F\cos\alpha_1 + (x - x_0)\sin\alpha_1 = f\left(x_0 + (x - x_0)\cos\alpha_1 - F\sin\alpha_1\right) \tag{14}$$

where the expression $x_0 + (x - x_0)\cos\alpha_1 - F\sin\alpha_1$ in the first pair of parentheses on the right-hand-side of the equation is the argument of the function $f(x)$.

The five derivatives of $F(t,x)$ used in Eqn. (13) can be evaluated approximately as following:

$$\begin{aligned}
F_x &= f' - \tan\alpha_1 + O(F^3) \\
F_{xx} &= f'' + O(F^3) \\
F_t &= -\alpha_1'(x - x_0)\sec^2\alpha_1 + O(F^3) \\
F_{tx} &= -\alpha_1'\sec^2\alpha_1 + O(F^3) \\
F_{tt} &= -(x - x_0)\sec^2\alpha_1(\alpha_1'' + 2\alpha_1'^2\tan\alpha_1) + O(F^3)
\end{aligned} \tag{15}$$

where the $'$ denotes differentiation of $f(x)$ and $\alpha(t)$ with respect to x and t, respectively.

III. Integral Boundary-Layer Method

On consideration of computational cost as well as uncertainties of turbulence modeling involved in a finite difference method, we use an integral boundary-layer method to account for the viscous effect. The classical boundary-layer calculation is to solve the boundary-layer thickness using the boundary-layer edge pressure gradient obtained from the outer inviscid flow solver. However, it is well known that this so-called direct method of boundary-layer calculation breaks down for flows involving strong inviscid-viscous interactions, especially when separation exists. Thus we couple the inverse boundary-layer calculation with the outer inviscid flow solution. In an inverse boundary-layer calculation, on the other hand, the edge pressure or velocity is solved from a given distribution of boundary-layer displacement thickness. More conveniently, following Cater[19] , we introduce the perturbation mass flow parameter $\overline{m} = \rho_e U_e \delta^*$. For a given distribution of $\overline{m}$ along the wall, we solve the boundary-layer edge velocity U_e.

By definition, $\delta^* = H\theta$, so expanding $\frac{d\overline{m}}{ds} = \frac{d(\rho_e U_e H\theta)}{ds}$ we get:

$$\frac{1}{\overline{m}}\frac{d\overline{m}}{ds} = \frac{1}{H}\frac{dH}{ds} + \frac{1}{\theta}\frac{d\theta}{ds} + (1 - M_e^2)\frac{1}{U_e}\frac{dU_e}{ds} \tag{16}$$

where δ and θ are the boundary-layer displacement and momentum thicknesses; ρ_e, U_e and M_e are local air density, velocity and Mach number at the boundary-layer edge, respectively; s is the streamwise coordinate along the airfoil wall or wake; H is the boundary-layer shape factor.

Considering the correlation between the shape factor H and the kinematic shape factor $\overline{H}$, i.e. $H = R_1(\overline{H} + 1) - 1$, we have:

$$\frac{dH}{ds} = R_1\frac{d\overline{H}}{ds} + (H + 1)\frac{R_3}{U_e}\frac{dU_e}{ds} \tag{17}$$

Thus eqn. (16) becomes:

$$\frac{H\theta}{\overline{m}}\frac{d\overline{m}}{ds} = H\frac{d\theta}{ds} + R_1\theta\frac{d\overline{H}}{ds} + [(H+1)R_3 + H(1-M_e^2)]\frac{\theta}{U_e}\frac{dU_e}{ds} \tag{18}$$

Here, R_1, R_2 , and R_3 are three parameters defined for convenience which are related to the ratio of specific heats γ, temperature recovery factor r, and the local boundary-layer edge Mach number M_e :

$$\begin{aligned} R_1 &= 1 + \frac{\gamma-1}{2} r M_e^2 \\ R_2 &= 1 + \frac{\gamma-1}{2} M_e^2 \\ R_3 &= \frac{(\gamma-1) r M_e^2 R_2}{R_1} \end{aligned} \tag{19}$$

For a turbulent boundary-layer , Head[20] introduced the entrainment coefficient C_E, which stands for the rate at which fluid from the outer inviscid flow enters the boundary-layer through the boundary-layer edge. By definition,

$$C_E = \frac{1}{\rho_e U_e}\frac{d(\rho_e U_e H_1 \theta)}{ds} \tag{20}$$

where H_1 is Head's shape factor. Again, expanding the derivative we get:

$$C_E = H_1\frac{d\theta}{ds} + H_1(1-M_e^2)\frac{\theta}{U_e}\frac{dU_e}{ds} + \theta\frac{dH_1}{d\overline{H}}\frac{d\overline{H}}{ds} \tag{21}$$

In addition, we have the integral momentum equation for compressible boundary-layer:

$$\frac{C_f}{2} = \frac{d\theta}{ds} + (H + 2 - M_e^2)\frac{\theta}{U_e}\frac{dU_e}{ds} \tag{22}$$

Thus we obtain a linear system of equations (18,21,22) about three unknown derivatives : $\frac{d\theta}{ds}$, $\frac{dU_e}{ds}$, and $\frac{d\overline{H}}{ds}$. Solving it, we have now a system of three first-order ordinary differential equations about three boundary-layer parameters: θ, U_e, and $\overline{H}$.

In addition, we employ Green's lag equation[16] to account for the history effects in nonequilibrium turbulent boundary-layer:

$$\begin{aligned} \theta\frac{dC_E}{ds} &= \overline{F}\left\{\frac{2.8}{H+H_1}\left[(C_\tau)_{EQ0}^{0.5} - \lambda(C_\tau)^{0.5}\right]\right. \\ &\quad \left. - \left[1 + 0.075M_e^2\frac{R_1}{1+0.1M_e^2}\right]\frac{\theta}{U_e}\frac{dU_e}{ds} + \left(\frac{\theta}{U_e}\frac{dU_e}{ds}\right)_{EQ}\right\} \end{aligned} \tag{23}$$

Here, C_τ is the shear stress coefficient, λ is a parameter to account for secondary effects, $\overline{F}$ is another parameter to be defined in the Appendix. The subscript EQ denotes quantities evaluated under equilibrium conditions where the shape factor and the entrainment coefficient are invariant, while $EQ0$ denotes quantities evaluated under equilibrium flow free of secondary effects.

Therefore, totally we have a system of four first-order ordinary differential equations for the four unknown boundary-layer parameters . Given a distribution of $\overline{m}$ along the wall plus the initial values at a starting point such as a fixed transition point, we can integrate the four ordinary differential equations using Runge-Kutta method and solve for the four unknown boundary-layer parameters: θ, U_e, $\overline{H}$, and C_E. As for correlations of various parameters in the four equations, i.e. C_f, F, H_1, C_τ, $(\frac{\theta}{U_e}\frac{dU_e}{ds})_{EQ}$, and $(C_\tau)_{EQ0}^{0.5}$, etc., we follow those in Green's paper[16] . For completeness, we list them in the Appendix.

IV. Inviscid-Viscous Coupling Procedure

Given the boundary-layer edge properties obtained from the outer inviscid solver, we can use Thwaites' method[21] to calculate the laminar part of the boundary-layer starting from the stagnation point. Transition is either specified or determined using Michel's formula[22] :

$$Re_\theta > 1.174(1 + \frac{22400}{Re_s})Re_s^{0.46} \tag{24}$$

For the turbulent part, the boundary-layer calculation needs to be coupled with the outer Equivalent Inviscid Flow(EIF) calculation. We employ Carter's "semi-inverse" coupling scheme[23] . We first guess a distribution of the boundary-layer displacement thickness δ^*. Using ρ_e and U_e from a preliminary inviscid calculation, we obtain a guessed perturbation mass-flow parameter $\overline{m} = \rho_e U_e \delta^*$. An inverse boundary-layer calculation following the last section gives us a viscous version of the boundary-layer edge velocity U_{ev}. Also from $\overline{m}$, we can derive the wall and wake boundary-conditions for the EIF calculation. Solving the Euler equations with these boundary-conditions for the outer EIF, we have an inviscid version of boundary-layer edge velocity U_{ei}. Then we can use Carter's relaxation scheme[23] to get an updated guess of the boundary-layer thickness:

$$\frac{\delta^*_{new}}{\delta^*_{old}} = 1 + \omega(\frac{U_{ev}}{U_{ei}} - 1) \tag{25}$$

Here, ω is an under-relaxation factor. Convergence is judged from the difference between the two boundary-layer edge velocities U_{ev} and U_{ei} . Two orders-of-magnitude drop of the difference between these two velocities over the inviscid one is enough for most of cases.

As we solve the Euler equations for the outer EIF, we need four boundary-conditions from the matching requirements of the EIF with the viscous flow for a 2D problem. However, as Sockol and Johnston[24] proved, if we use the surface normal blowing velocity derived from the continuity equation as a boundary condition, then other matching requirements such as the normal flux of streamwise momentum and total enthalpy will automatically be satisfied. Considering a first-order boundary-layer approximation, we can simply calculate the surface values of density, streamwise velocity and total enthalpy via linear extrapolation from the adjacent grid to the wall. Therefore the only change in solving the EIF is that we need to add a blowing velocity in Eqn. (10). The blowing velocity can be obtained from mass conservation:

$$V_n = \frac{1}{\rho_e}\frac{d}{ds}(\rho U_e \delta^*) = \frac{1}{\rho_e}\frac{d}{ds}(\overline{m}) \tag{26}$$

It is known that the Kutta condition is automatically satisfied in Euler calculations. So in the wake, unlike the boundary-layer coupling with a potential code, we do not need to use a jump condition. We simply treat the wake as two boundary-layers developed on both sides of the dividing streamline of the wake. Currently we assume this dividing streamline is the extension of the airfoil mean chord rather than calculating it accurately.

V. Results and Discussions

A. Steady Flows

In order to validate the proposed interactive boundary-layer method, we first test it for two steady cases. One is for the airfoil NACA0012 at $M = 0.775$ and $\alpha = 2.05$; the other for the supercritical airfoil RAE2822 at $M = 0.750$ and $\alpha_{exp} = 3.19$ (the corrected value $\alpha_c = 2.81$ is used in our calculation). Figure 1 shows the comparisons of the calculated and experimental surface pressures for both cases. The results obtained from the current interactive boundary-layer method agree with experimental data very well. The shock position is shifted forward and the strength weakened compared to the pure inviscid solutions.

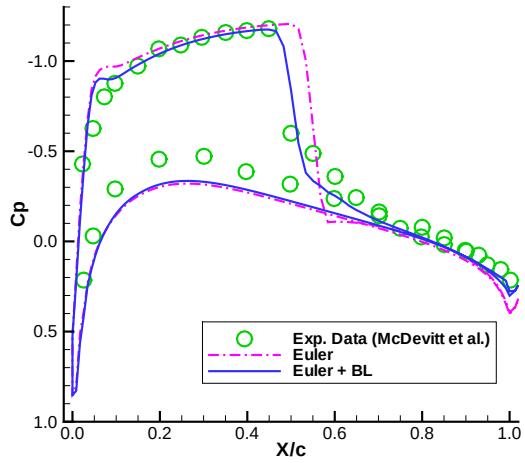

(a) NACA0012 airfoil at $M = 0.775$, $\alpha = 2.05^o$, $Re_c = 10^7$

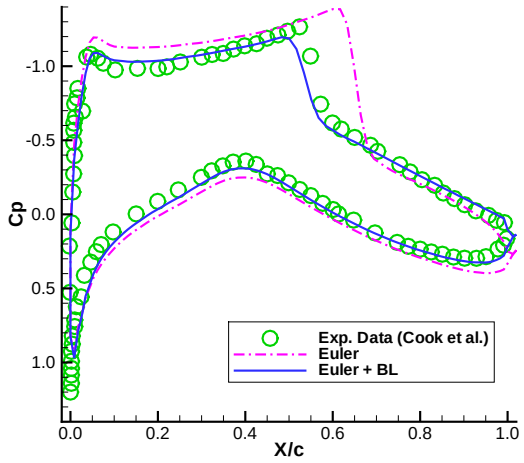

(b) RAE2822 airfoil at $M = 0.750$, $\alpha = 2.81^o$, $Re_c = 6.2 \times 10^6$

Figure 1. Comparison of calculated and experimental pressure coefficient.

B. Unsteady Flows

The unsteady Euler equations are solved by a dual-time stepping method. The time derivative terms in the boundary-layer equation are neglected in the current formulation. Consequently, the coupling of the boundary-layer in unsteady calculations is in a quasi-steady manner. At every real time step, we take the final boundary-layer displacement thickness from the previous real time step as the initial guess and start boundary-layer coupling process for the current time step. In this way, for every real time step, about 5 times of boundary-layer coupling can achieve enough convergence. We choose an unsteady case of NACA64A010 airfoil in pitching motion around its quarter-chord point. Experimental data were provided by Davis[25] . The pitching motion of the airfoil is described by the following equation.

$$\alpha(t) = \alpha_m + \alpha_0 \sin \omega t \tag{27}$$

where α is the instantaneous angle of attack; ω, α_m, and α_0 are constants. The angular frequency ω is related to the reduced frequency defined as

$$\kappa = \frac{\omega c}{2U_\infty} \tag{28}$$

The calculations start from the uniform flow of velocity U_∞ as an initial solution. After three periods of the airfoil motion an essentially periodic solution is obtained. In this paper six periods of motion are computed to ensure periodic solution.

In the test case , the free stream Mach number is $M_\infty = 0.796$, and the mean angle of attack $\alpha_m = 0.0^o$, the pitching amplitude $\alpha_0 = 1.01^o$, the reduced frequency $\kappa = 0.202$. The experimental Reynolds number based on airfoil chord is $Re_c = 13 \times 10^6$. The computed instantaneous pressure distributions with and without boundary-layer coupling at the eight phase angles during the sixth cycle of motion are compared with the experimental data in Figure 2. The eight phase angles are 0, 45, 90, 135, 180, 225, 270, and 315 degrees. The time variation of the computed and experimental data of the surface pressure distributions

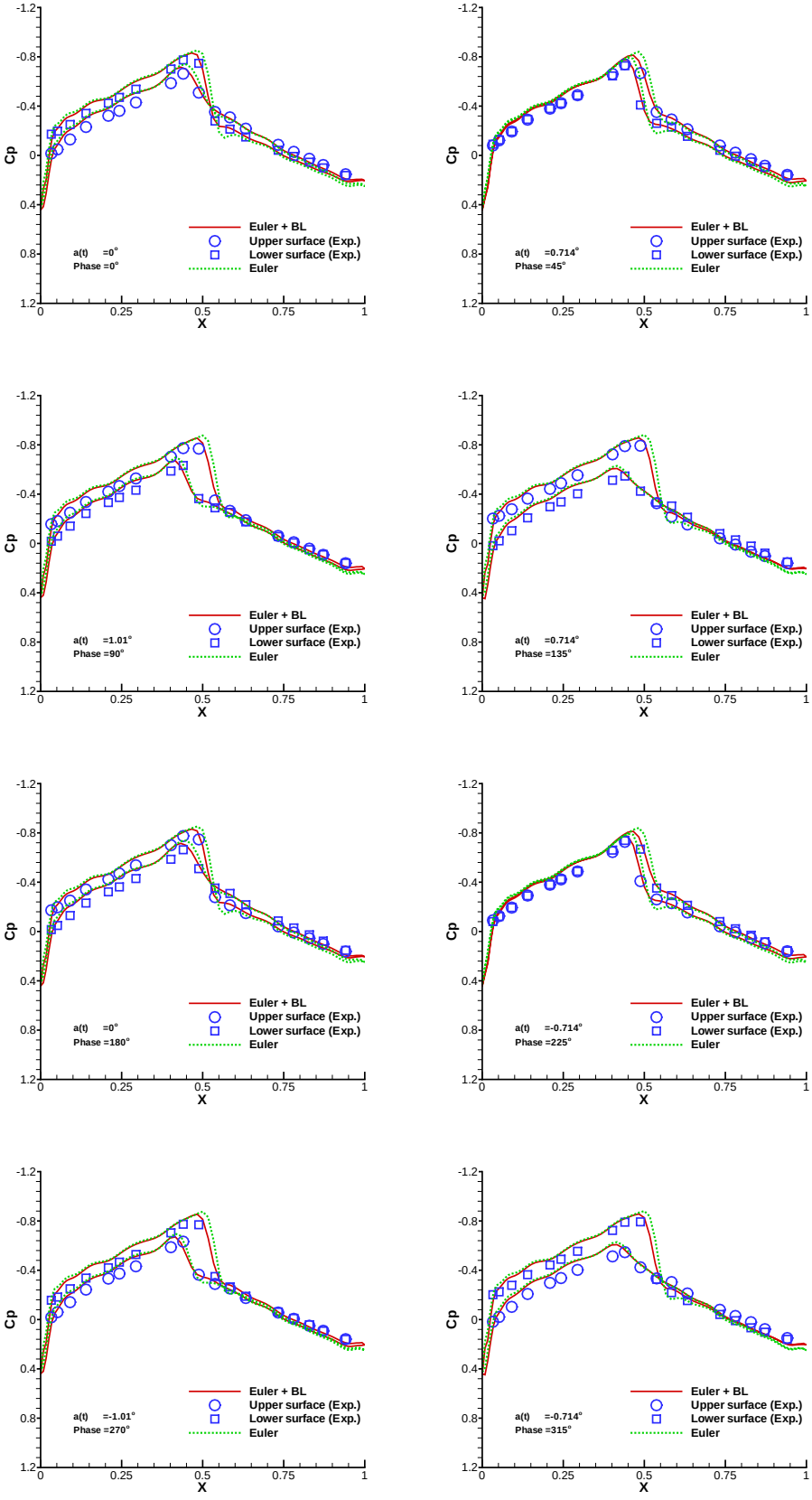

Figure 2. Comparison of calculated surface pressure distributions with and without boundary-layer coupling, and experiment, NACA64A010, $M_\infty = 0.796$, $\alpha_m = 0.0^o$, $\alpha_0 = 1.01^o$, $\kappa = 0.202$, $Re = 13 \times 10^6$.

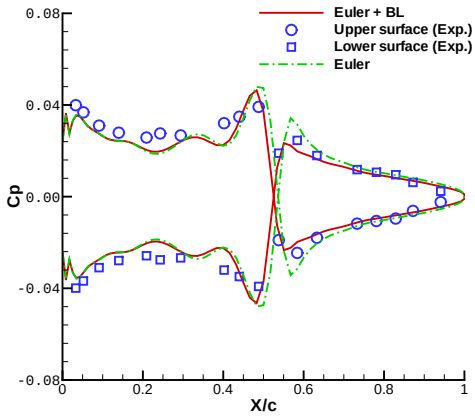

(a) Real component, first mode

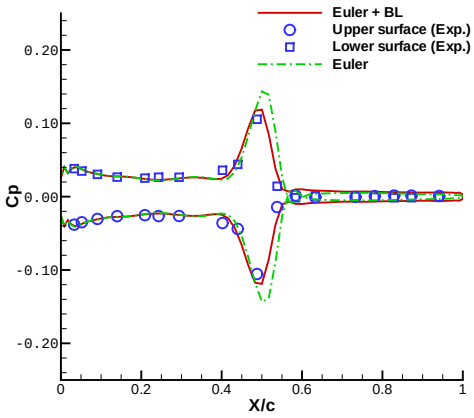

(b) Imaginary component, first mode

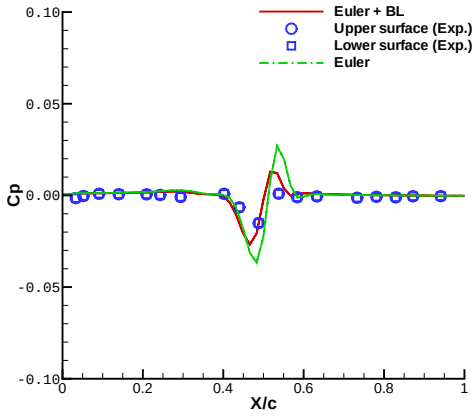

(c) Real component, second mode

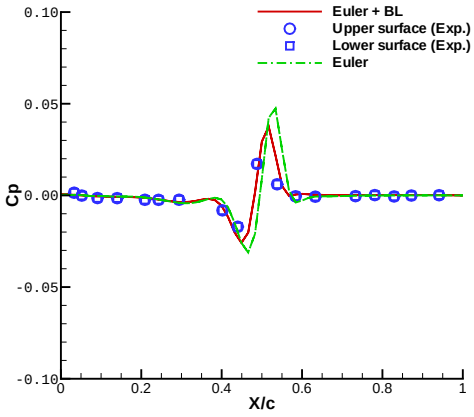

(d) Imaginary component, second mode

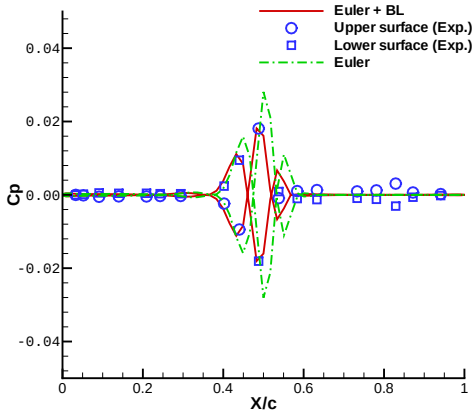

(e) Real component, third mode

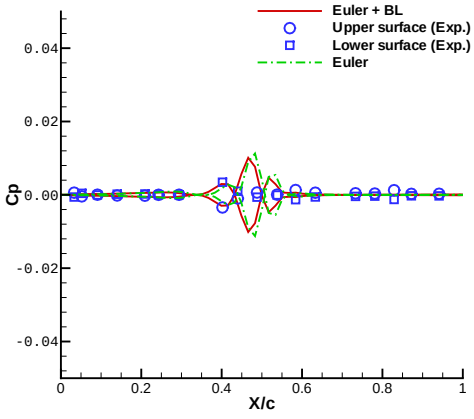

(f) Imaginary component, third mode

Figure 3. Comparison of calculated Fourier Components of surface pressure variations with and without boundary-layer coupling, and experiment, NACA64A010, $M_\infty = 0.796$, $\alpha_m = 0.0^o$, $\alpha_0 = 1.01^o$, $\kappa = 0.202$, $Re = 13 \times 10^6$.

can be expressed in terms of their Fourier components. Figure 3 shows the comparison of the real and imaginary parts of the first three Fourier modes of the unsteady pressure coefficient over the airfoil surface. The solutions with boundary-layer coupling in general give better prediction of shock position and strength compared to the experimental data.

C. Flutter Calculations

After the validation of the current interactive boundary-layer method by steady and unsteady calculations, we test its capability for the prediction of flutter in a coupled CFD-CSD approach.[4] The two-dimensional Isogai wing model,[26,27] Case A ($\mu = 60$) is tested. This model simulates the bending and torsional motion of a wing cross-section in the outboard portion of a swept wing. It consists of two degrees of freedom, plunging and pitching, for a NACA 64A010 airfoil. The details of the structural model can be found in Reference 28 as well as in Refs. 26 and 27. Gao et al.[29] have already predicted the flutter boundary for this model using the Cartesian Euler solver mentioned earlier. We compare the results from the current interactive boundary-layer method with theirs as well as thin-layer Navier-Stokes(TLNS) results provided by Prananta et al.[30] In our calculations, we use $Re = 6 \times 10^6$ as Prananta et al.[30]

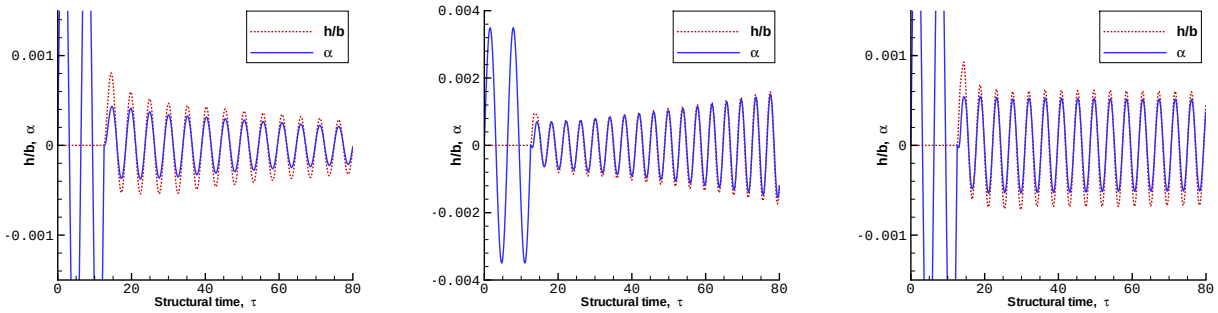

(a) $V_f = 1.60$, stable situation. (b) $V_f = 2.15$, unstable situation. (c) $V_f = 1.92$, neutral situation.

Figure 4. Time histories of the pitching and plunging amplitudes for $M_\infty = 0.885$.

For flutter calculation, two cycles of forced pitching are performed first and then the airfoil is free to move by itself. Figure 4 shows the flutter computational results for the Isogai wing model at a flight Mach number of 0.885. Plotted in the figure are the time histories of the pitching and plunging amplitudes computed by the integrated CFD-CSD code using the current interactive boundary-layer method. The flutter speed index V_f is defined as

$$V_f = \frac{U_\infty}{b\omega\sqrt{\mu}}$$

where ω is the eigen frequency of the structure. As show in the figure, for low $V_f = 1.60$, both the pitching and plunging amplitudes decay with time, indicating that the aeroelastic system is stable for this particular condition. At a higher V_f, the system may become less and less stable until one or both of the pitching and plunging motions diverge when $V_f = 2.15$. In between these two V_f conditions, there is a particular point where the system is neutrally stable. The figure shows this happens when $V_f = 1.92$.

A converging point and a diverging point like the above are first identified, from which we can interpolate the V_f in between to obtain an estimate of the neutral point. We then perform a computation with the new V_f to see if it is above or below the stability limit, or perhaps right at the neutral point. It may take several runs for a given free-stream Mach number before the V_f corresponding to the neutral stability point can be accurately located by this "bi-section" method. With this method computations for a number of

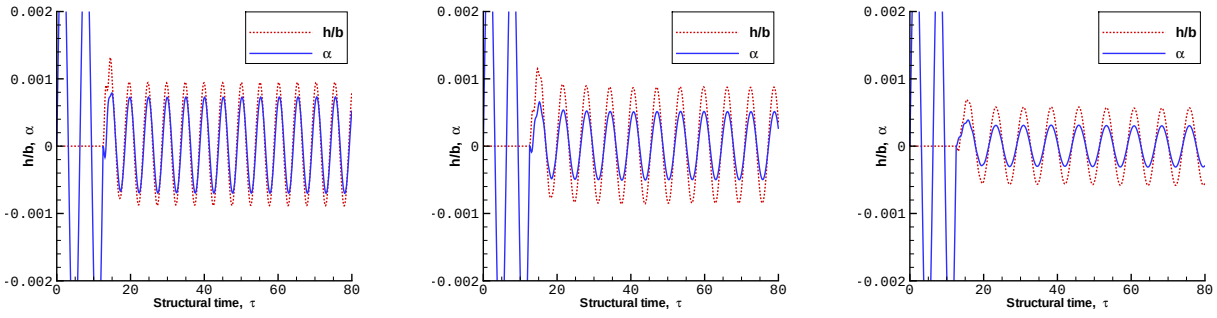

(a) $M = 0.750$, $V_f = 1.24$ (b) $M = 0.800$, $V_f = 0.85$ (c) $M = 0.860$, $V_f = 0.63$

(d) $M = 0.870$, $V_f = 0.96$ (e) $M = 0.875$, $V_f = 1.55$ (f) $M = 0.905$, $V_f = 2.34$

Figure 5. Time histories of the pitching and plunging amplitudes at neutral points.

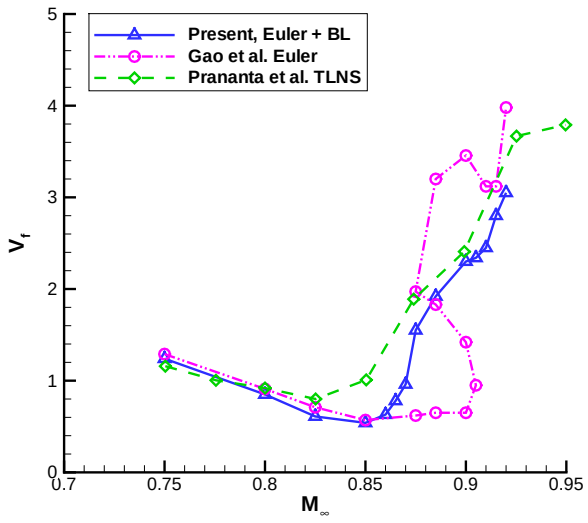

Figure 6. Computed flutter boundary for the Isogai wing model.

free-stream Mach numbers for the Isogai wing model are performed. Figure 5 shows the time responses at the neutral points for some mach numbers. The flutter boundary predicted by the present boundary-layer coupling method is compared in Figure 6 with those predicted by Gao et al.[29] and Prananta et al.[30]

The inviscid results show an obvious S shape. That means in the transonic region there are more than one flutter boundary for some particular Mach numbers. For example, as Gao et al.[29] predicted, at $M_\infty = 0.885$, the system initially crosses the stability boundary at $V_f = 0.65$ to become unstable as V_f increases. As V_f increases above 1.83, however, the system becomes stable again until V_f reaches above 3.20 when it returns to being unstable. Nonetheless, in our boundary-layer coupling calculation, there is not such a curving back phenomenon. For each Mach number, only one flutter-boundary point is obtained just like the TLNS results. The boundary-layer coupling code predicts the boundary a little bit lower than the inviscid prediction until $M = 0.85$. After that, it predicts the flutter boundary much higher than the boundary by Gao et al.[29] Basically, the current interactive boundary-layer method predicts the flutter boundary close to the TLNS results except for the dip where the biggest difference exists. Without experimental data, we can not yet conclude whether the TLNS results or our results are more accurate.

VI. Conclusions

This paper presents an efficient interactive boundary-layer method capable of aeroelastic simulations. Euler equations on stationary Cartesian grids are solved for the inviscid part and coupled with an integral boundary-layer code. It is shown that the results obtained using this interactive boundary-layer method agree well with experimental data for both steady and unsteady cases. Computation of the 2D Isogai wing model shows significantly different behavior of the flutter boundary when viscous effect is included. The current interactive boundary-layer method predicts the flutter-boundary close to the results from a thin-layer Navier-Stokes method.

Appendix

For the Runge-Kutta integration of the four ordinary differential equations in the inverse boundary-layer calculation, we need correlations for those parameters in the equations. We follow the correlations presented in Green's paper[16] and list them here:

$$Re_\theta = \frac{\rho_e U_e \theta}{\mu_e}$$

$$F_c = (1 + \frac{\gamma - 1}{2} M_e^2)^{0.5}, \; F_R = 1 + 0.056 M_e^2$$

$$C_{f0} = (\frac{0.01013}{log_{10}(F_R Re_\theta) - 1.02} - 0.00075)/F_c$$

$$\frac{\overline{H}}{\overline{H}_0} = \overline{H} \left\{ 1 - 6.55 \left[\frac{C_{f0}}{2} (1 + 0.04 M_e^2) \right]^{0.5} \right\}$$

$$C_f = C_{f0} \left\{ 0.9 (\frac{\overline{H}}{\overline{H}_0} - 0.4)^{-1} - 0.5 \right\}$$

$$H = (\overline{H} + 1) \left(1 + \frac{\gamma - 1}{2} r M_e^2 \right) - 1$$

$$H_1 = 3.15 + \frac{1.72}{\overline{H} - 1} - 0.01 (\overline{H} - 1)^2$$

$$\overline{F} = \frac{0.02 C_E + C_E^2 + 0.8 C_{f0}/3}{0.01 + C_E}$$

$$C_\tau = (0.024 C_E + 1.2 C_E^2 + 0.32 C_{f0})(1 + 0.1 M_e^2)$$

$$\left(\frac{\theta}{U_e} \frac{dU_e}{dx} \right)_{EQ0} = \frac{1.25}{H} \left[\frac{C_f}{2} - \left(\frac{\overline{H} - 1}{6.432 \overline{H}} \right)^2 (1 + 0.04 M_e^2)^{-1} \right]$$

$$(C_E)_{EQ0} = H_1 \left[\frac{C_f}{2} - (H + 1) \left(\frac{\theta}{U_e} \frac{dU_e}{dx} \right)_{EQ0} \right]$$

$$(C_\tau)_{EQ0} = (0.024 (C_E)_{EQ0} + 1.2 (C_E)_{EQ0}^2 + 0.32 C_{f0})(1 + 0.1 M_e^2)$$

$$C = (C_\tau)_{EQ0} (1 + 0.1 M_e^2)^{-1} \lambda^{-2} - 0.32 C_{f0}$$

$$(C_E)_{EQ} = (C/1.2 + 0.0001)^{0.5} - 0.01$$

$$\left(\frac{\theta}{U_e} \frac{dU_e}{dx} \right)_{EQ} = \left[\frac{C_f}{2} - \frac{(C_E)_{EQ}}{H_1} \right] / (H + 1)$$

Here, λ is a parameter to account for secondary influences such as wall curvature. Currently we ignore those secondary influences and thus set $\lambda = 1$ on the airfoil wall . However in the wake, we set $\lambda = 0.5$ as well as $C_f = C_{f0} = 0$ as suggested by Green.[16]

Acknowledgement

This work is supported by NASA Langley Research Center, contract number NAG-1-02050.

References

[1]Rodden, W. P. and Johnson, E. H., *MSC/NASTRAN Aeroelastic Analysis User's Guide, Version 68*, The Macneal-Schwender Corporation, Los Angeles, 1994.

[2]Lee-Rausch, E. M. and Batina, J. T., "Wing Flutter Boundary Prediction Using Unsteady Euler Aerodynamic Method," *Journal of Aircraft*, Vol. 32, No. 2, Mar.-Apr. 1995, pp. 416–422.

[3]Lee-Rausch, E. M. and Batina, J. T., "Wing Flutter Computations Using an Aerodynamic Model Based on the Navier-Stokes Equations," *Journal of Aircraft*, Vol. 33, No. 6, Nov.-Dec. 1996, pp. 1139–1147.

[4]Liu, F., Cai, J., Zhu, Y., Wong, A. S. F., and Tsai, H.-M., "Calculation of Wing Flutter by a Coupled Fluid-Structure Method," *Journal of Aircraft*, Vol. 38, No. 2, Mar.-Apr. 2001, pp. 334–342.

[5]Gibbons, M., "Aeroelastice Calculations Using CFD for a Typical Business Jet Model," NASA CR 4753, 1996.

[6]Bartels, R., "Flow and Turbulence Modeling and Computation of Shock Buffet Onset for Conventional and Supercritical Airfoils," NASA TP 1998-206908, 1998.

[7]Tang, L., Bartels, R., Chen, P., and Liu, D. D., "Numerical Investigation of Transonic Limit Oscillations of a 2-D supercritical Wing," AIAA Paper 2001-1290, 2001.

[8]Batina, J. T., "A Finite-Difference Approximate-Factorization Algorithm for Solution of the Unsteady Transonic Small-Disturbance Equation," NASA TP 3129, Jan. 1992.

[9]Edwards, J., "Transonic Shock Oscillations Calculated with a New Interactive Boundary Layer Coupling Method," AIAA Paper 93-0777, 1993.

[10]Edwards, J., "Transonic Shock Oscillations and Wing Flutter Calculated with an Interactive Boundary Layer Coupling Method," *EUROMECH-Colloquium 349, Simulation of Fluid-Structure Interaction in Aeronautics*, Gottingen, Germany, Sept. 1996.

[11]Whitfield, D., Swafford, T., and Jacocks, J., "Calculation of Turbulent Boundary Layers with Separation and Viscous-Inviscid Interaction," *AIAA Journal*, Vol. 19, No. 10, 1981, pp. 1315–1322.

[12]Lee, T. J., *Transonic Viscous-Inviscid Interaction Using Euler and Inverse Boundary-Layer Equations*, Ph.D. dissertation, Mississippi State Univ., Dec. 1983.

[13]Giles, M., Drela, M., and Thompkins, W. T., "Newton Solution of Direct and Inverse Transonic Euler Equations," AIAA Paper 85–1530, AIAA 7th Computational Fluid Dynamics Conference, Cincinnati, Ohio, June 1985.

[14]Beaumiera, P., Arnaudb, G., and Castellinb, C., "Performance prediction and flow field analysis of rotors inhover using a coupled Euler/boundary layer method," *Aerosp.Sci.Technol*, , No. 3, 1999, pp. 473–484.

[15]Gao, C., Luo, S., and Liu, F., "Calculation of Unsteady Transonic Flow by an Euler Method with Small Perturbation Boundary Conditions," AIAA Paper 2003-1267, Jan. 2003.

[16]Green, J. E., Weeks, D. J., and Brooman, J. W. F., "Prediction of Turbulent Boundary Layers and Wakes in Compressible Flow by a Lag-Entrainment Method," British Aeronautical Research Council R & M 3791, 1977.

[17]Jameson, A., "Time dependent calculations using multigrid, with applications to unsteady flows past airfoils and wings," AIAA Paper 91–1596, June 1991, 10th AIAA Computational Fluid Dynamics Conference.

[18]Jameson, A., Schmidt, W., and Turkel, E., "Numerical Solutions of the Euler Equations by Finite Volume Methods Using Runge-Kutta Time-Stepping Schemes," AIAA Paper 81–1259, June 1981.

[19]Vatsa, V. and Carter, J., "Development of an Integral Boundary-Layer Technique for Separated Turbulent Flow," United Technologies Research Center Report UTRC81-28, 1981.

[20]Head, M., "Entrainment in the turbulent boundary layer," A.R.C.R.&M. 3152, 1958.

[21]Thwaites, B., "Approximate Calculation of the Laminar Boundary Layer," *Aeronaut. Q.*, Vol. 1, No. 6, 1949, pp. 245–280.

[22]Michel, R., "Etude de la Transition sur les Profiles d'Aile," ONERA Report 1/1578A, 1951.

[23]Carter, J. E., "A New Boundary-Layer Inviscid Iteration Technique for Separated Flow," AIAA Paper 1979-1450, 1979.

[24]Sockol, P. M. and Johnston, W. A., "Coupling Conditions for Integrating Boundary Layer and Rotational Inviscid Flow," *AIAA Journal*, Vol. 24, No. 6, June 1986, pp. 1033–1035.

[25]Davis, S. S., "NACA64A010 Oscillatory Pitching," Compendium of Unsteady Aerodynamics Measurements, AGARD Report 702, 1982.

[26]Isogai, K., "On the Transonic-Dip Mechanism of flutter of a Sweptback Wing," *AIAA Journal*, Vol. 17, No. 7, July 1979, pp. 793–795.

[27]Isogai, K., "On the Transonic-Dip Mechanism of flutter of a Sweptback Wing: Part II," *AIAA Journal*, Vol. 19, No. 9, Sept. 1981, pp. 1240–1242.

[28]Alonso, J. J. and Jameson, A., "Fully-Implicit Time-Marching Aeroelastic Solutions," AIAA Paper 94–0056, Jan. 1994.

[29]Gao, C., Luo, S., Liu, F., and Schuster, D. M., "Calculation of Airfoil Flutter by an Euler Method with Approximate Boundary Conditions," AIAA Paper 2003-3830, June 2003.

[30]Prananta, B. B., L., H. M. H., and J., Z. R., "Two-Dimensional Transonic Aeroelastic Analysis Using Thin-Layer Navier-Stokes Method," *Journal of Fluid and Structures*, Vol. 12, 1998, pp. 655–676.